RSC Advances

COMMUNICATION

View Article Online
View Journal | View Issue

Cite this: *RSC Adv.*, 2015, **5**, 24872

Received 7th February 2015
Accepted 3rd March 2015

DOI: 10.1039/c5ra02427g

www.rsc.org/advances

Synthesis of $CaCO_3$@C yolk–shell particles for CO_2 adsorption†

Yash Boyjoo,[a] Kelly Merigot,[b] Jean-François Lamonier,[c] Vishnu K. Pareek,[a] Moses O. Tade[a] and Jian Liu*[a]

We report the synthesis of $CaCO_3$@C yolk–shell particles with a microporous carbon shell through a selective etching method. The $CaCO_3$@C exhibits an enhanced CO_2 adsorption, relative to the porous $CaCO_3$ nanoparticles or the porous carbon shell, with a capacity of 19.30 cm^3 STP g^{-1} (0.86 mmol g^{-1} or 31.64 cm^3 STP cm^{-3} sorbent) under ambient conditions (23 ± 1 °C and 1 atm CO_2).

Yolk–shell nanoparticles are materials with nanoparticle cores inside hollow shells. They are promising functional nanomaterials with various functionalities both on the core and shell, which can have a wide variety of applications such as catalysis, drug/gene delivery, energy storage, biosensors, and Raman scattering (SERS) technologies.[1–3] Various yolk–shell nanoparticles (YSNs) with different chemical compositions have been reported such as metal NPs@SiO_2, metal oxide@SiO_2, metal NPs@C, metal NPs@metal oxide, metal NPs@polymer, SiO_2@metal oxide, SiO_2@C and polymer@polymer[2,4–11] by using different synthetic methods, for example, a soft templating method and selective etching methods. To date, most of the reported YSNs are limited to silica, polymer, carbon and a few metal oxides.[2,12–14] To enrich the YSNs library and meet the requirements of practical applications, synthesis of YSNs with a new composition is desirable.

Porous carbons with various morphologies and structures have been widely investigated for CO_2 adsorption and separation[15] due to their large surface areas, ease of synthesis, low-cost, and high stability.[15–19] The synthesis of porous carbon aerogels and xerogels *via* resorcinol–formaldehyde (RF) resins has been extensively reported.[16,20–24] Taking the advantages of yolk–shell structures, such as large void space for accommodating of guest molecules, different functionality of both core and shell, constructing yolk–shell particle with porous carbon shell would be very promising for design of CO_2 capture and conversion nanoreactors. Calcium-based materials (calcium oxide, calcium hydroxide, and calcium carbonate) have been proved as excellent sorbents for high temperature CO_2 capture,[25] however, their adsorption performance quickly declines with multiple reuse due to irreversible particle sintering and agglomeration at high temperatures.[26,27]

We herein report the first example for the synthesis of $CaCO_3$@C yolk–shell particles. The features offered by these particles are: high surface area and pore volume, basic calcium-based core for affinity of CO_2, large void space for CO_2 storage, and microporous carbon shell[28] for preferential passage of small molecules with respect to larger sized molecules.[29] These yolk–shell particles could find application as a catalyst support (*e.g.*, nano-metals) or in drug and gene delivery for biomedical applications,[30] or high temperature CO_2 capture.

As illustrated in Scheme 1, a four-step synthetic process was employed by using $CaCO_3$ particles as core materials. First, a silica layer was coated around the $CaCO_3$ nanospheres by a Stöber method to obtain $CaCO_3$@SiO_2 core–shell particles. Next, the $CaCO_3$@SiO_2 was coated with a RF resin *via* a modified Stöber method[28] to produce $CaCO_3$@SiO_2@RF core–shell–shell particles. This was followed by a carbonisation process under N_2 flow, which converted the RF resin into a microporous carbon shell to produce $CaCO_3$@SiO_2@C. Finally, the silica layer was removed with the treatment of hot concentrated NaOH. The detailed experimental procedures are presented in the ESI.†

$CaCO_3$ nanospheres were prepared by the rapid mixing of solutions of $CaCl_2$ and Na_2CO_3 containing surfactant poly(4-styrenesulfonic acid) sodium salt (PSS). The as-synthesised $CaCO_3$ nanospheres have an average particle size of 450 nm as demonstrated by SEM image (Fig. 1a). The particle size distribution of the $CaCO_3$ spheres (Fig. 1b) further confirms the uniformity of the porous $CaCO_3$ particles. The successful preparation of $CaCO_3$@SiO_2 as well as $CaCO_3$@SiO_2@C from $CaCO_3$ nanospheres was tracked and confirmed by TEM

[a]*Department of Chemical Engineering, Curtin University, Perth, WA 6845, Australia. E-mail: jian.liu@curtin.edu.au*

[b]*Department of Physics, Curtin University, Perth, WA 6845, Australia*

[c]*Université de Lille 1, Unité de Catalyse et Chimie du Solide, UMR CNRS 8181, 59652 Villeneuve d'Ascq, France*

† Electronic supplementary information (ESI) available: Materials and methods, SEM and TEM images, CO_2 adsorption data. See DOI: 10.1039/c5ra02427g

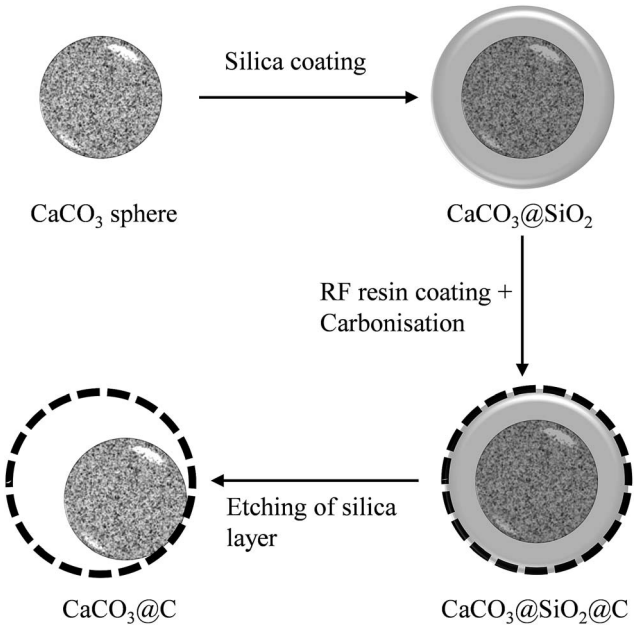

Scheme 1 Steps involved in the synthesis of $CaCO_3$@C yolk–shell particles.

characterization as shown in Fig. 2a–d. Fig. 3a and b show the SEM and TEM images of the obtained $CaCO_3$@C yolk–shell particles. The presence of a movable core inside a thin carbon shell can be easily identified from the SEM images *via* the particles with broken shells, exposing the core. The TEM image shows a yolk–shell particle with a porous $CaCO_3$ core and a golf ball like porous carbon shell. The size of the core and hollow space is *ca.* 240 nm and 310 nm in diameter, respectively, and the carbon shell's thickness is around 10 nm. High angle annular dark field scanning transmission electron microscopy (HAADF-STEM) and energy dispersive X-ray spectroscopy (EDX) of the particles are shown in Fig. 3c–f, which indicates the formation of a carbon shell outside the calcium carbonate core.

XRD pattern of the $CaCO_3$@C yolk–shell particles (Fig. 3g) further confirms that the main composition of the core is $CaCO_3$. A small amount of CaO and $CaSiO_3$ (due to reaction of CaO with un-removed SiO_2) is also present. Interestingly, when the $CaCO_3$ precursor nanoparticles were subjected to the same calcination conditions as with the yolk–shell particles, a $Ca(OH)_2$ phase was formed (according to the XRD data, Fig. S1†) due to the loss of CO_2 resulting from the continuous supply of fresh N_2 in the furnace at 600 °C for a long period (4 hours). This suggests that the nanoporous SiO_2 layer prevent the escape of the large CO_2 molecules during carbonation of $CaCO_3$@SiO_2@RF core–shell–shell particles. As a result, the retainment of CO_2 gas within the SiO_2 layer led to an expansion of the space between the nanocrystals inside the core, increasing its porosity by creating channels and bridges, compared to the $CaCO_3$ precursor nanoparticles (this can be seen by comparing Fig. 2a and d). Furthermore, some of CaO formed at the edge of the core reacted with SiO_2 (that could not be removed by NaOH etching) to form $CaSiO_3$. The porosity of the $CaCO_3$@C yolk–shell particles were measured by nitrogen sorption, which revealed a type IV isotherm indicating their mesoporous structures[31] (Fig. 3h). The pore size distribution curve in Fig. S2† shows that the material is highly microporous to mesoporous in nature. The high microporosity of the yolk–shell particles is due to the carbon shell.[28] The BET surface area, density and total pore volume of the $CaCO_3$@C YSNs are 381 $m^2\ g^{-1}$, 0.12 g cm^{-3} and 0.61 $cm^3\ g^{-1}$, respectively, while those of the $CaCO_3$ precursor nanoparticles are 89 $m^2\ g^{-1}$, 0.63 g cm^{-3} and 0.14 $cm^3\ g^{-1}$, respectively (see Fig. S3† for N_2 sorption isotherm and pore size distribution of the $CaCO_3$ precursor).

In order to control: (1) the hollow space inside shell and (2) the thickness of shell, the synthesis parameters such as silica precursor concentration and RF ratio were varied, respectively (see Fig. S4–S6 in ESI†). It was found that the general size of the hollow space and shell thickness increased when increasing the silica precursor concentration and the RF ratio, respectively. In addition, by increasing the etching time, as shown in Fig. 4, the hollow space increases and the porous $CaCO_3$ core gets more exposed due to the removal of the silica layer around the core. The ability to control these physical parameters is important in terms of improving the mechanical strength of the particles, and tuning its functionalities.

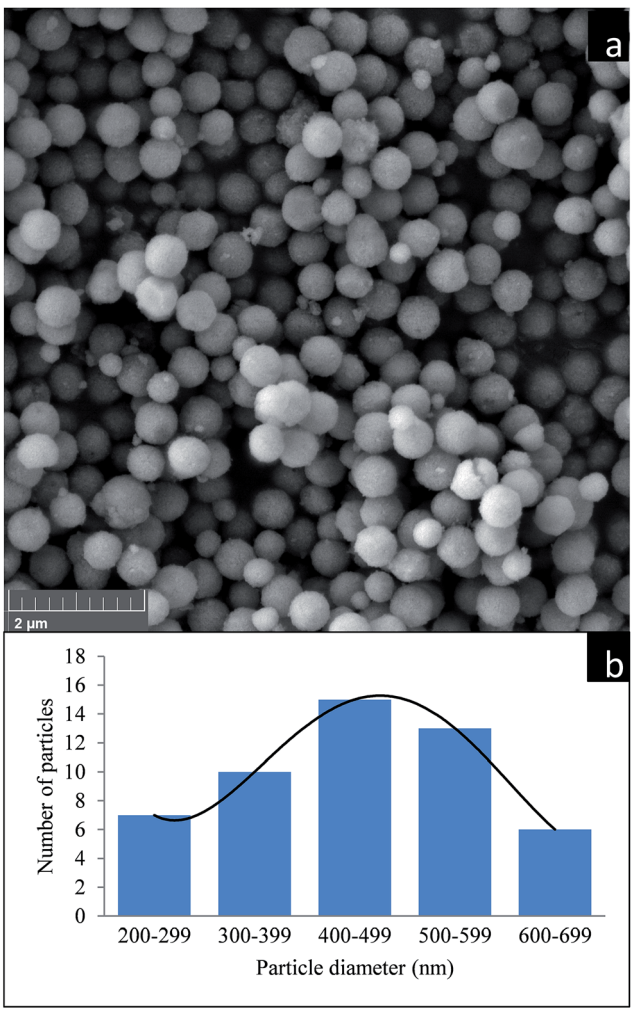

Fig. 1 (a) SEM of synthesised $CaCO_3$ nano-spheres and (b) particle size distribution of synthesised $CaCO_3$ nano-spheres.

For further optimisation and confirmation of the core compositions, TGA of $CaCO_3$ precursor nanoparticles was performed as shown in Fig. S7,† from which it can be seen that the $CaCO_3$ decomposes to CaO between ~600 °C and ~780 °C. As a result, the effect of high temperature recalcination on the $CaCO_3$@C yolk–shell particles was investigated. Fig. S8† shows the XRD patterns for $CaCO_3$@C samples recalcined under N_2 for 1 hour at 650 °C, 700 °C and 750 °C, respectively. At 650 °C, a CaO peak starts to appear and becomes more prominent at 700 °C. However, when the temperature is further increased to 750 °C, a $CaSiO_3$ phase forms due to reaction of CaO with remaining SiO_2 on the core surface. Hence it is shown that the phase and composition of the core can be changed from $CaCO_3$ to mixture of $CaCO_3$ and CaO, further to $CaSiO_3$ by simply tuning the recalcination temperature of the $CaCO_3$@C yolk–shell particles. The presence of CaO in the core increases its basicity, which can be an attractive characteristic for catalytic applications requiring basic conditions or high temperature CO_2 capture.

Developing a low cost and high efficient adsorbent for CO_2 capture is highly desirable in order to alleviate the crisis of climate change and greenhouse effect. Fig. 5 shows the CO_2 adsorption isotherms for the $CaCO_3$ precursor nanoparticles, $Ca(OH)_2$ (calcined $CaCO_3$ precursor) particles, $CaCO_3$@SiO_2@C and $CaCO_3$@C yolk–shell particles. The original $CaCO_3$ shows a relatively low adsorption capacity (6.30 cm^3 STP g^{-1} or 45.00 cm^3 STP cm^{-3} sorbent at 23 ± 1 °C and 1 atm CO_2) even at higher CO_2 pressures due to weak physisorption of the gas on the particles. The adsorption capacity of $CaCO_3$@SiO_2@C is

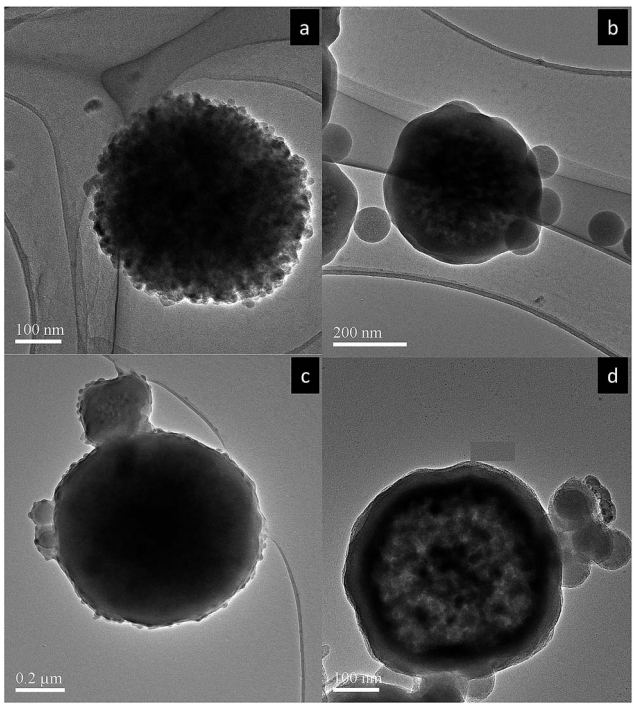

Fig. 2 TEM images for tracking the steps in synthesis of $CaCO_3$@C: (a) $CaCO_3$ particle, (b) $CaCO_3$@SiO_2 particle, (c) $CaCO_3$@SiO_2@RF particle and (d) $CaCO_3$@SiO_2@C particle. TEOS concentration = 4 mL g^{-1} $CaCO_3$, RF ratio = 0.5.

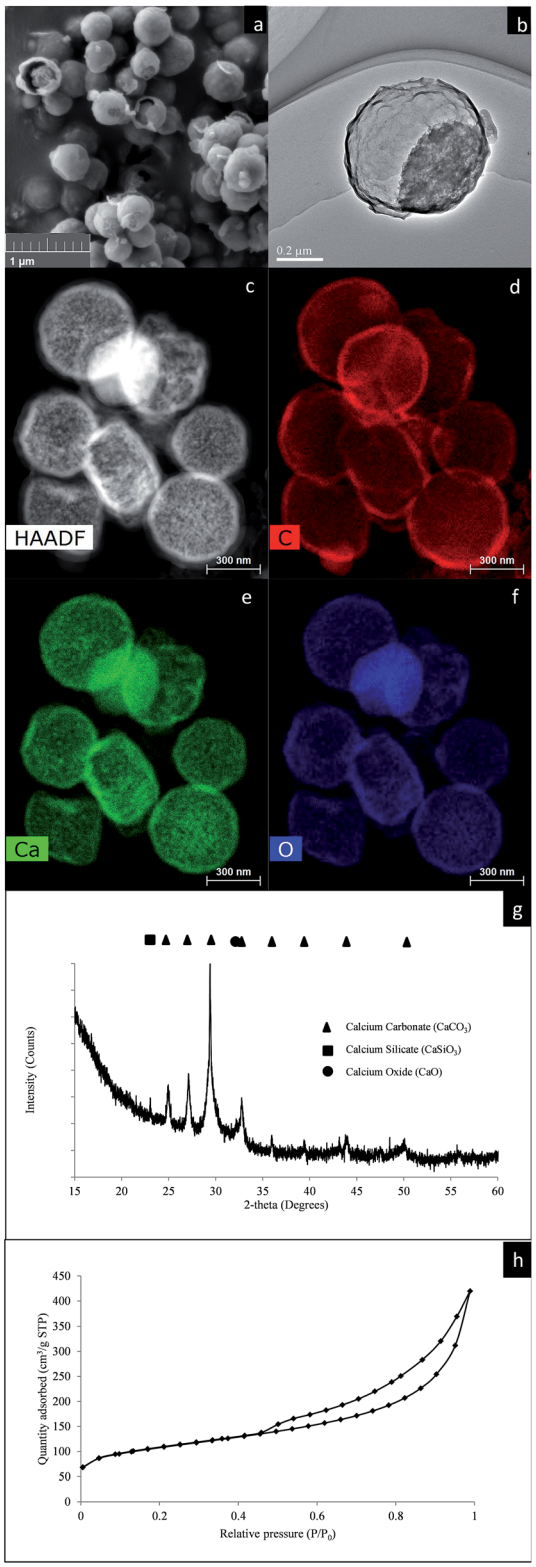

Fig. 3 (a) SEM, (b) TEM, (c) HAADF-STEM images, (d–f) EDX elemental mapping of carbon, calcium and oxygen respectively, (g) XRD analysis and (h) N_2 adsorption isotherm for the $CaCO_3$@C yolk–shell particles. TEOS concentration = 2 mL g^{-1} $CaCO_3$, RF ratio = 0.5 and etching time = 3 hours.

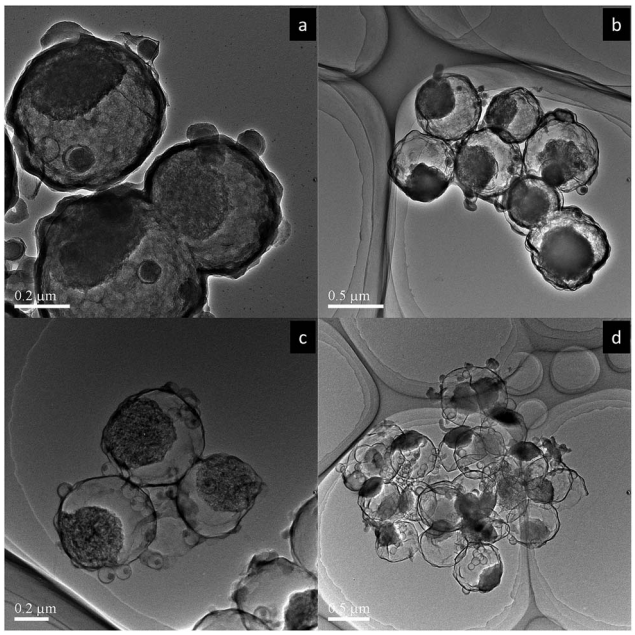

Fig. 4 Effect of etching time on $CaCO_3$@C particles; (a) $t = 1$ hour, (b) $t = 2$ hours, (c) $t = 3$ hours and (d) $t = 4$ hours. TEOS concentration = 4 mL g^{-1} $CaCO_3$, RF ratio = 0.5.

even lower (4.50 cm^3 STP g^{-1} sorbent at 23 ± 1 °C and 1 atm CO_2) due to the impervious layer of SiO_2 which hindered CO_2 penetration towards the $CaCO_3$ core; hence physisorption was mostly achieved on the surface of the carbon shell. The calcined precursor, $Ca(OH)_2$ particles had the lowest CO_2 adsorption capacity at 0.40 cm^3 STP g^{-1} sorbent (at 23 ± 1 °C and 1 atm CO_2), probably due to the loss in surface area resulting from particles agglomeration at high calcination temperature. However, the improvement in the CO_2 uptake is obvious with the yolk–shell particles due to removal of the SiO_2 layer for CO_2 adsorption. The $CaCO_3$ core of $CaCO_3$@C was more porous than the $CaCO_3$ precursor (as can be seen by comparing Fig. 2a and d). Furthermore, the core–shell architecture allowed each $CaCO_3$ core to be completely surrounded by a CO_2 atmosphere

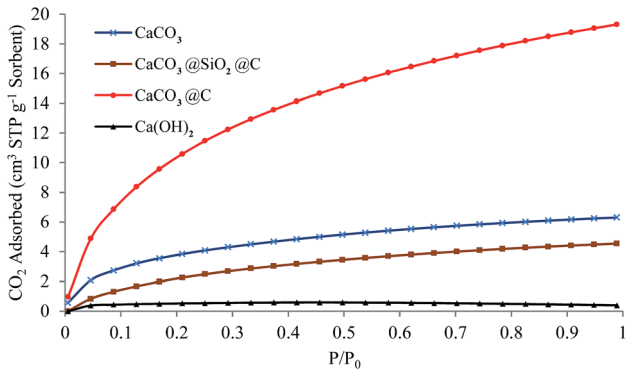

Fig. 5 CO_2 adsorption isotherms ($T = 23 \pm 1$ °C) for $CaCO_3$ precursor nanoparticles, $CaCO_3$@SiO_2@C particles, $CaCO_3$@C yolk–shell particles and $Ca(OH)_2$ particles. For the core–shell–shell and yolk–shell particles, TEOS concentration = 6 mL g^{-1} $CaCO_3$, RF ratio = 0.5 and etching time = 3 hours.

for enhanced adsorption. The maximum amount of CO_2 adsorbed with $CaCO_3$@C at ambient conditions (23 ± 1 °C and 1 atm CO_2) is 19.30 cm^3 STP g^{-1} sorbent (0.86 mmol g^{-1} or 31.64 cm^3 STP cm^{-3} sorbent). The volumetric capacity of $CaCO_3$ based sorbents is comparable with other adsorbents such as activated carbon,[15] much higher than high surface area zeolite 13X (with 5.00 cm^3 STP cm^{-3}).[32] Fig. S9† shows the determination of the optimum etching time according to CO_2 adsorption isotherms. It was found that 3 hours of NaOH etching was enough to expose the $CaCO_3$ core for optimum CO_2 adsorption. The CO_2 adsorption amount is due to the physisorption, which follows the sequence of $CaCO_3$@C > $CaCO_3$ precursor nanoparticles > $CaCO_3$@SiO_2@C > $Ca(OH)_2$ particles, indicating that the combination of $CaCO_3$ core, hollow space and carbon shells is favourable for high CO_2 adsorption at low temperature.

Conclusions

$CaCO_3$@C yolk–shell particles have been successfully synthesised by a selective etching method. The yolk–shell structures exhibited enhanced CO_2 uptake of 19.3 cm^3 STP g^{-1} (0.862 mmol g^{-1} or 31.64 cm^3 STP cm^{-3} sorbent) at 23 ± 1 °C under 1 atm CO_2, compared with 6.3 cm^3 STP g^{-1} for the original $CaCO_3$ core, or 4.5 cm^3 STP g^{-1} for the porous carbon shell. This was due to the relatively high surface area and pore volume, as well as the hollow space of the yolk–shell particle. It was shown that the core composition of the yolk–shell particles can be varied from $CaCO_3$, CaO, or $CaSiO_3$ by simply tuning the recalcination temperature. These yolk–shell particles with porous calcium-based materials core and microporous carbon shell make them potentially attractive materials for environmental remediation (SO_x, NO_x removal), biomedical applications and nanocatalysis. Further investigation on the high temperature adsorption of CO_2, SO_x is ongoing.

Acknowledgements

The authors acknowledge the facilities, scientific and technical assistance of the Curtin University Electron Microscope Laboratories, a facility partially funded by the University, State and Commonwealth Governments. The authors also wish to acknowledge the facilities, and the scientific and technical assistance of the Australian Microscopy & Microanalysis Research Facility at the Centre for Microscopy, Characterisation & Analysis, The University of Western Australia, a facility funded by the University, State and Commonwealth Governments. JL gratefully acknowledges the support of France-Australia Science Innovation Collaboration (FASIC) program Early Career Fellowships.

Notes and references

1 J. Liu, S. Z. Qiao, S. Budi Hartono and G. Q. M. Lu, *Angew. Chem.*, 2010, **122**, 5101–5105.
2 J. Liu, S. Z. Qiao, J. S. Chen, X. W. D. Lou, X. Xing and G. Q. M. Lu, *Chem. Commun.*, 2011, **47**, 12578–12591.

3 J. Liu, H. Q. Yang, F. Kleitz, Z. G. Chen, T. Yang, E. Strounina, G. Q. M. Lu and S. Z. Qiao, *Adv. Funct. Mater.*, 2012, **22**, 591–599.
4 X. Fang, S. Liu, J. Zang, C. Xu, M.-S. Zheng, Q.-F. Dong, D. Sun and N. Zheng, *Nanoscale*, 2013, **5**, 6908–6916.
5 C. Galeano, C. Baldizzone, H. Bongard, B. Spliethoff, C. Weidenthaler, J. C. Meier, K. J. J. Mayrhofer and F. Schüth, *Adv. Funct. Mater.*, 2014, **24**, 220–232.
6 Y. J. Hong, M. Y. Son and Y. C. Kang, *Adv. Mater.*, 2013, **25**, 2279–2283.
7 J. Wang, W. Li, F. Wang, Y. Xia, A. M. Asiri and D. Zhao, *Nanoscale*, 2014, **6**, 3217–3222.
8 T. Yang, J. Liu, Y. Zheng, M. J. Monteiro and S. Z. Qiao, *Chem.–Eur. J.*, 2013, **19**, 6942–6945.
9 T. Yang, R. Zhou, D. Wang, S. P. Jiang, Y. Yamauchi, S. Qiao, M. Monteiro and J. Liu, *Chem. Commun.*, 2015, **51**, 2518–2521.
10 R. Liu, F. Qu, Y. Guo, N. Yao and R. D. Priestley, *Chem. Commun.*, 2014, **50**, 478–480.
11 R. Liu, Y.-W. Yeh, V. H. Tam, F. Qu, N. Yao and R. D. Priestley, *Chem. Commun.*, 2014, **50**, 9056–9059.
12 Y. Chen, H.-R. Chen and J.-L. Shi, *Acc. Chem. Res.*, 2013, **47**, 125–137.
13 J. Lee, S. M. Kim and I. S. Lee, *Nano Today*, 2014, **9**, 631–667.
14 M. Priebe and K. M. Fromm, *Chem.–Eur. J.*, 2015, **21**, 3854–3874.
15 A. H. Lu and S. Dai, *Porous Materials for Carbon Dioxide Capture*, Springer, 2014.
16 M. Antonietti, N. Fechler and T.-P. Fellinger, *Chem. Mater.*, 2013, **26**, 196–210.
17 A.-H. Lu, W.-C. Li, G.-P. Hao, B. Spliethoff, H.-J. Bongard, B. B. Schaack and F. Schüth, *Angew. Chem., Int. Ed.*, 2010, **49**, 1615–1618.
18 A.-H. Lu, T. Sun, W.-C. Li, Q. Sun, F. Han, D.-H. Liu and Y. Guo, *Angew. Chem., Int. Ed.*, 2011, **50**, 11765–11768.
19 S. Soll, T.-P. Fellinger, X. Wang, Q. Zhao, M. Antonietti and J. Yuan, *Small*, 2013, **9**, 4135–4141.
20 Z.-L. Yu, Z.-Y. Wu, S. Xin, C. Qiao, Z.-Y. Yu, H.-P. Cong and S.-H. Yu, *Chem. Mater.*, 2014, **26**, 6915–6918.
21 W. Kiciński and A. Dziura, *Carbon*, 2014, **75**, 56–67.
22 D. Wu, C. M. Hui, H. Dong, J. Pietrasik, H. J. Ryu, Z. Li, M. Zhong, H. He, E. K. Kim and M. Jaroniec, *Macromolecules*, 2011, **44**, 5846–5849.
23 S. A. Al-Muhtaseb and J. A. Ritter, *Adv. Mater.*, 2003, **15**, 101–114.
24 V. G. Pol, L. K. Shrestha and K. Ariga, *ACS Appl. Mater. Interfaces*, 2014, **6**, 10649–10655.
25 Y. Boyjoo, V. K. Pareek and J. Liu, *J. Mater. Chem. A*, 2014, **2**, 14270–14288.
26 A. Samanta, A. Zhao, G. K. Shimizu, P. Sarkar and R. Gupta, *Ind. Eng. Chem. Res.*, 2011, **51**, 1438–1463.
27 J. Wang, L. Huang, R. Yang, Z. Zhang, J. Wu, Y. Gao, Q. Wang, D. O'Hare and Z. Zhong, *Energy Environ. Sci.*, 2014, 3478–3518.
28 N. Li, Q. Zhang, J. Liu, J. Joo, A. Lee, Y. Gan and Y. Yin, *Chem. Commun.*, 2013, **49**, 5135–5137.
29 N. P. Wickramaratne and M. Jaroniec, *ACS Appl. Mater. Interfaces*, 2013, **5**, 1849–1855.
30 Y. Zhao, Z. Luo, M. Li, Q. Qu, X. Ma, S.-H. Yu and Y. Zhao, *Angew. Chem., Int. Ed.*, 2015, **54**, 919–922.
31 A. W. Adamson and A. P. Gast, *Physical chemistry of surfaces*, Wiley, 1997.
32 J. Garcia-Martinez, *Nanotechnology for the Energy Challenge*, Wiley-VCH, 2013.

